

# Inpainting of Cyclic Data using First and Second Order Differences

Ronny Bergmann\*, Andreas Weinmann†

February 12, 2018

## Abstract

Cyclic data arise in various image and signal processing applications such as interferometric synthetic aperture radar, electroencephalogram data analysis, and color image restoration in HSV or LCh spaces. In this paper we introduce a variational inpainting model for cyclic data which utilizes our definition of absolute cyclic second order differences. Based on analytical expressions for the proximal mappings of these differences we propose a cyclic proximal point algorithm (CPPA) for minimizing the corresponding functional. We choose appropriate cycles to implement this algorithm in an efficient way. We further introduce a simple strategy to initialize the unknown inpainting region. Numerical results both for synthetic and real-world data demonstrate the performance of our algorithm.

**Keywords.** Inpainting, variational models with higher order differences, cyclic data, phase-valued data, cyclic proximal point algorithm.

## 1 Introduction

Image inpainting is a frequently arising problem in image processing. Examples are restoring scratches in photographs, removal of superimposed objects, dealing with areas removed by a user, digital zooming, edge decoding, restoration of defects in audio/video recordings or in seismic data. The term ‘inpainting’ first appeared in [6], but earlier work on disocclusions was already done, e.g., in [13, 38]. In this respect also interpolation, approximation, and extrapolation problems may be viewed as inpainting problems. Inpainting is a very active field of research which has been tackled by various approaches. For a good overview we refer to the (tutorial) papers [10, 12, 17, 30]. While exemplar-based and sparsity-based (dictionary/frame/tensor) methods are in general better suited for filling large texture areas, diffusion-based and corresponding variational techniques show good results for natural images. The total variation (TV) regularized model proposed in [45] for denoising was first applied to inpainting in [4, 15]. It was later also used in combination with other methods, however,

---

\*Department of Mathematics, Technische Universität Kaiserslautern, Paul-Ehrlich-Str. 31, 67663 Kaiserslautern, Germany, bergmann@mathematik.uni-kl.de.

†Department of Mathematics, Technische Universität München and Fast Algorithms for Biomedical Imaging Group, Helmholtz-Zentrum München, Ingolstädter Landstr. 1, 85764 Neuherberg, Germany, andreas.weinmann@tum.de.

the TV regularizer typically introduces a staircasing effect in the corresponding minimizer. A simple method to avoid these artifacts consists in the incorporation of second order derivatives into the model. Indeed, starting with [14] various approaches with higher order derivatives have been proposed, see, e.g., [9, 16, 19, 31, 33, 35, 40, 46, 47, 48, 51]. In this paper, we address the problem of inpainting cyclic data using a variational model with second order cyclic differences. In general, manifold-valued data processing has recently gained a lot of interest. Examples are wavelet-type multiscale transforms for manifold data [29, 42, 52] and manifold-valued partial differential equations [18, 28]. Also statistical issues on Riemannian manifolds have been considered [22, 23, 41], in particular the statistics of circular data [21, 32].

**Related work.** Although very popular for processing images with scalar and vector-valued data, TV minimization has only very recently been applied to cyclic structures. From a theoretical point of view TV functionals for manifold-valued functions have been studied in [26, 27]. These papers extend the previous work [25] on  $\mathbb{S}^1$ -valued functions where, in particular, the existence of minimizers of certain energies is shown in the space of functions with bounded total cyclic variation. First order TV minimization for cyclic data in image processing has been investigated in [49, 50]. The authors unwrap the data to the real line and propose an algorithm based on functional lifting which takes the periodicity into account. In particular, they also consider cyclic inpainting. An algorithm for TV minimization on Riemannian manifolds was proposed in [34]. The approach is based on a reformulation as a multilabel optimization problem with an infinite number of labels. Using convex relaxation techniques, the resulting hard optimization problem is approximated which also requires the discretization of the manifold. Another approach for denoising manifold-valued data via first order TV minimization was given in [53]. The authors propose cyclic and parallel proximal point algorithms which will also be our method of choice.

**Contributions.** We propose two models for inpainting of cyclic data using first and second order absolute cyclic differences. In our preprint [5] we introduced absolute second order differences for cyclic data in a sound way. We further deduced analytical expressions for the proximal mappings of these differences. Here, our first model considers the noise free inpainting situation, whereas the second one handles simultaneously inpainting and denoising. The variational formulations allow for the decomposition of the whole functionals into simpler ones, for each of which the proximal mappings are given explicitly. Thus, the minimizers can be computed efficiently by a cyclic proximal point method. We propose a suitable initialization of the inpainting area. We demonstrate by numerical examples the strength of our algorithm. Compared to [49, 50] we neither have to employ Fréchet means nor to discretize the manifold.

**Organization.** In Sec. 2 we introduce our absolute second order cyclic differences and provide analytical expressions for their proximal mappings. Then, in Sec. 3, we introduce our inpainting model and propose a procedure to initialize the unknown inpainting region. Sec. 4 describes the cyclic proximal point algorithm. Finally, Sec. 5 contains numerical examples. Conclusions and directions of future work are given in Sec. 6.

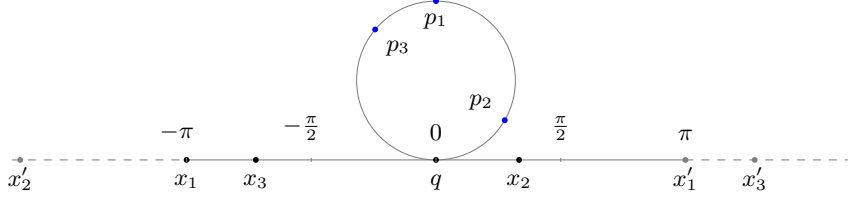


**Figure 1.** Three points  $p_j$ ,  $j = 1, 2, 3$ , on the circle and their possible unwrappings  $x_1, x_2, x_3 \in [-\pi, \pi)$  with respect to the origin  $q$  and other possibilities  $x'_2, x_1, x_3$  and  $x_2, x_3, x'_1$  that correspond to the same situation on  $\mathbb{S}^1$ . These are taken into account for  $d(x; w)$ .

## 2 Absolute First and Second Order Cyclic Differences and Their Proximal Mappings

Let  $\mathbb{S}^1 := \{p_1^2 + p_2^2 = 1 : p = (p_1, p_2)^T \in \mathbb{R}^2\}$  be the unit circle endowed with the *geodesic distance*  $d_{\mathbb{S}^1}(p, q) := \arccos(\langle p, q \rangle)$ . Given a base point  $q \in \mathbb{S}^1$ , the *exponential map*  $\exp_q : \mathbb{R} \rightarrow \mathbb{S}^1$  from the tangent space  $T_q\mathbb{S}^1 \simeq \mathbb{R}$  of  $\mathbb{S}^1$  at  $q$  onto  $\mathbb{S}^1$  is defined by

$$\exp_q(x) = R_x q, \quad R_x := \begin{pmatrix} \cos x & -\sin x \\ \sin x & \cos x \end{pmatrix}.$$

This map is  $2\pi$ -periodic, i.e.,  $\exp_q(x) = \exp_q((x)_{2\pi})$  for any  $x \in \mathbb{R}$ , where  $(x)_{2\pi}$  denotes the unique point in  $[-\pi, \pi)$  such that  $x = 2\pi k + (x)_{2\pi}$ ,  $k \in \mathbb{Z}$ . For  $p, q \in \mathbb{S}^1$  with  $\exp_q(0) = q$ , there is a unique  $x \in [-\pi, \pi)$  satisfying  $\exp_q(x) = p$ . Given such representants  $x_j \in [-\pi, \pi)$  of  $p_j \in \mathbb{S}^1$ ,  $j = 1, 2$  centered at an arbitrary base point  $q \in \mathbb{S}^1$  the geodesic distance becomes

$$d_{\mathbb{S}^1}(p_1, p_2) = d(x_1, x_2) = \min_{k \in \mathbb{Z}} |x_2 - x_1 + 2\pi k| = |(x_2 - x_1)_{2\pi}|$$

which is of course independent of  $q$ . We want to define higher order differences for points  $(p_j)_{j=1}^d \in (\mathbb{S}^1)^d$  using their representants  $x := (x_j)_{j=1}^d \in [-\pi, \pi)^d$ . To achieve independence of the base point the differences must be shift invariant modulo  $2\pi$ , see Fig. 1. Let  $1_d$  denote the vector with  $d$  entries 1. We define the *absolute cyclic difference* of  $x \in [-\pi, \pi)^d$  with respect to a difference filter  $w \in \mathbb{R}^d$  with  $\langle w, 1_d \rangle = 0$  by

$$d(x; w) := \min_{\alpha \in \mathbb{R}} \langle [x + \alpha 1_d]_{2\pi}, w \rangle, \quad (1)$$

where  $[x]_{2\pi}$  denotes the componentwise application of  $(t)_{2\pi}$  if  $t \neq (2k + 1)\pi$ ,  $k \in \mathbb{Z}$  and  $[(2k + 1)\pi]_{2\pi} = \pm\pi$ ,  $k \in \mathbb{Z}$ . Let

$$b_1 := (-1, 1)^T \quad \text{and} \quad b_2 := (1, -2, 1)^T, \quad b_{1,1} := (-1, 1, 1, -1)^T$$

be a first order (forward) difference filter, and two second order difference filters, respectively. For  $w \in \mathcal{B} := \{b_1, b_2, b_{1,1}\}$  we have shown in our accompanying preprint [5] that the absolute cyclic differences can be rewritten as

$$d(x; w) = (\langle x, w \rangle)_{2\pi}. \quad (2)$$

Clearly, we have  $d(x; b_1) = d(x_1, x_2)$ . Interestingly, the definition (1) and (2) do not coincide, e.g., for third order cyclic differences [5].

Next we are interested in proximal mappings of absolute cyclic differences. Recall that for a proper, closed, convex function  $\varphi : \mathbb{R}^N \rightarrow (-\infty, +\infty]$  and  $\lambda > 0$  the *proximal mapping*  $\text{prox}_{\lambda\varphi} : \mathbb{R}^N \rightarrow \mathbb{R}^N$  is well defined by

$$\text{prox}_{\lambda\varphi}(f) := \arg \min_{x \in \mathbb{R}^N} \frac{1}{2} \|f - x\|_2^2 + \lambda\varphi(x).$$

We introduce the proximal mapping  $\text{prox}_{\lambda d(\cdot; w)} : (\mathbb{S}^1)^d \rightarrow (\mathbb{S}^1)^d$  by

$$\text{prox}_{\lambda d(\cdot; w)}(f) := \arg \min_{x \in [-\pi, \pi]^d} \frac{1}{2} \sum_{j=1}^d d(x_j, f_j)^2 + \lambda d(x; w), \quad \lambda > 0.$$

The following theorem determines the proximal mapping analytically for  $w \in \mathcal{B}$ . In particular, the mapping is single-valued for  $f \in [-\pi, \pi]^d$  with  $|(\langle f, w \rangle)_{2\pi}| < \pi$  and two-valued for  $|(\langle f, w \rangle)_{2\pi}| = \pi$ . Note that for  $w = b_1$  the second case appears exactly if  $f_1$  and  $f_2$  are antipodal points. For a proof we refer to our preprint [5].

**Theorem 2.1.** *For  $w \in \mathcal{B}$  set  $s := \text{sgn}(\langle f, w \rangle)_{2\pi}$ . Let  $f \in [-\pi, \pi]^d$ , where  $d$  is adapted to the respective length of  $w$ ,  $\lambda > 0$ , and  $m := \min \left\{ \lambda, \frac{|(\langle f, w \rangle)_{2\pi}|}{\|w\|_2^2} \right\}$ .*

*i) If  $|(\langle f, w \rangle)_{2\pi}| < \pi$ , then  $\text{prox}_{\lambda d(\cdot; w)}(f) = (f - s m w)_{2\pi}$ .*

*ii) If  $|(\langle f, w \rangle)_{2\pi}| = \pi$ , then  $\text{prox}_{\lambda d(\cdot; w)}(f) = \{(f + s m w)_{2\pi}, (f - s m w)_{2\pi}\}$ .*

For handling noisy data we will further need the following proximal mapping:

**Theorem 2.2.** *For  $f, g \in [-\pi, \pi]^N$  we have*

$$\begin{aligned} \text{prox}_{\lambda d(\cdot, f)}(g) &:= \arg \min_x \sum_{j=1}^N (d(g_j, x_j)^2 + \lambda d(f_j, x_j)^2) \\ &= \left( \frac{g + \lambda f}{1 + \lambda} + \frac{\lambda}{1 + \lambda} 2\pi v \right)_{2\pi}, \end{aligned}$$

where  $d(g, f) := \sum_{j=1}^N d(g_j, f_j)$  and  $v = (v_j)_{j=1}^N \in \mathbb{R}^N$  is defined by

$$v_j := \begin{cases} 0 & \text{if } |g_j - f_j| \leq \pi, \\ \text{sgn}(g_j - f_j) & \text{if } |g_j - f_j| > \pi. \end{cases}$$

### 3 Inpainting Models for Cyclic data

Given an image domain  $\Omega_0 = \{1, \dots, N\} \times \{1, \dots, M\}$ , the inpainting region  $\Omega \subset \Omega_0$  is the subset where the pixel values  $f_{i,j}$ ,  $(i, j) \in \Omega$  are unknown. The (noiseless) inpainting problem consists of finding a function  $x$  on  $\Omega_0$  from data  $f$  given on  $\bar{\Omega} = \Omega_0 \setminus \Omega$  such that  $x$  is a suitable extension of  $f$  to  $\Omega_0$ . Let  $d_2(x) := d(x; b_2)$  and  $d_{1,1}(x) := d(x; b_{1,1})$ . Our functional for inpainting of noiseless cyclic data reads

$$\begin{aligned} \arg \min_{x \in [-\pi, \pi]^{N,M}} & \alpha \text{TV}_1^\Omega(x) + \beta \text{TV}_2^\Omega(x) + \gamma \text{TV}_{1,1}^\Omega(x), \\ \text{s.t.} & \quad x_{i,j} = f_{i,j} \quad \text{for all } (i, j) \in \bar{\Omega}, \end{aligned} \tag{3}$$

where  $\alpha := (\alpha_1, \alpha_2, \alpha_2, \alpha_4)$ ,  $\beta := (\beta_1, \beta_2)$  and the restricted first and second order difference terms given by

$$\begin{aligned} \alpha \text{TV}_1^\Omega(x) &= \alpha_1 \sum_{(i,j)} d(x_{i,j}, x_{i+1,j}) + \alpha_2 \sum_{(i,j)} d(x_{i,j}, x_{i,j+1}) \\ &\quad + \frac{1}{\sqrt{2}} \left( \alpha_3 \sum_{(i,j)} d(x_{i,j}, x_{i+1,j+1}) + \alpha_4 \sum_{(i,j)} d(x_{i,j+1}, x_{i+1,j}) \right), \end{aligned}$$

$$\beta \text{TV}_2^\Omega(x) = \beta_1 \sum_{(i,j)} d_2(x_{i-1,j}, x_{i,j}, x_{i+1,j}) + \beta_2 \sum_{(i,j)} d_2(x_{i,j-1}, x_{i,j}, x_{i,j+1}),$$

and

$$\gamma \text{TV}_{1,1}^\Omega(x) = \gamma \sum_{(i,j)} d_{1,1}(x_{i,j}, x_{i+1,j}, x_{i,j+1}, x_{i+1,j+1}),$$

where the sums are taken only for those  $(i, j)$  for which at least one entry  $x_{a,b}$  in the corresponding differences is contained in  $\Omega$ . We use the notation TV since the model of the first order differences resembles an anisotropic TV model.

For the inpainting problem in the presence of noise the requirement of equality on  $\bar{\Omega}$  is replaced by  $x$  being an approximation of  $f$ :

$$\arg \min_{x \in [-\pi, \pi)^{N,M}} F_{\bar{\Omega}}(x; f) + \alpha \text{TV}_1(x) + \beta \text{TV}_2(x) + \gamma \text{TV}_{1,1}(x), \quad (4)$$

where

$$F_{\bar{\Omega}}(x; f) := \sum_{(i,j) \in \bar{\Omega}} d(x_{i,j}, f_{i,j})^2.$$

and the first and second order difference terms sum over all indices in  $\Omega_0$  now.

**Initialization of the inpainting region.** Since the inpainting problem does not possess a unique minimizer the initialization of the inpainting area is crucial. We present a method which is related to the idea of unknown boundary conditions used by Almeida and Figueiredo in [1]. It can also be viewed as an implicit version of the ordering method of pixels by adapted distance functions used by März in [36, 37]. To this end, we initialize  $x_{i,j} = f_{i,j}$  for  $(i, j) \in \bar{\Omega}$ . The other ones are considered as not initialized. We use first, second and mixed order differences  $d = d_1, d_2$  and  $d_{1,1}$  and let  $t \in \{1, 2, (1,1)\}$ . Let  $x := (x_{k_1}, \dots, x_{k_l})^\top$  be a set of points corresponding to a stencil of such a difference term  $d_t$ . If  $k_i \in \Omega$ ,  $i \in \{1, \dots, l\}$ , is the unique index such that  $x_{k_i}$  is not yet initialized, i.e., there is exactly one unknown point at  $k_i \in \Omega$  in  $x$ , we can initialize this value as follows. The minimal value for the absolute cyclic finite difference is  $0 = (\langle x, b_t \rangle)_{2\pi}$  and this equation provides an initial value for  $x_{k_i}$ . Such a situation of exactly one unknown index  $k_i$  always exists at the boundary of the initialized area.

## 4 Cyclic Proximal Point Algorithm

Since the proximal mappings of our absolute cyclic differences can be efficiently computed using their analytical expressions in Theorem 2.1 and Theorem 2.2, we suggest to apply a

cyclic proximal point algorithm to find a minimizer for the inpainting problem. Recently, the proximal point algorithm (PPA) on the Euclidean space [44] was extended to Riemannian manifolds of non-positive sectional curvature [20] and also to Hadamard spaces [2]. A cyclic PPA (CPPA) on the Euclidean space was given in [7, 8] and on Hadamard spaces in [3]. Unfortunately, one of the simplest manifolds that is not of Hadamard type is the circle  $\mathbb{S}^1$ . However, under certain assumptions we were able to prove the convergence of the CPPA to a minimizer of the denoising problem for cyclic data, see [5]. A similar proof can also be given for the inpainting problem. Indeed, we have observed convergence of our algorithm in all numerical tests.

In the CPPA the original function  $J$  is split into a sum  $J = \sum_{l=1}^c J_l$  and the proximal mappings of the functions  $J_l$  are applied in each iteration cycle, i.e.,

$$x^{(k+1)} = \text{prox}_{\lambda_k J_c} \left( \text{prox}_{\lambda_k J_{c-1}} \left( \dots \left( \text{prox}_{\lambda_k J_1} (x^{(k)}) \right) \right) \right).$$

For  $J = J_1 + J_2$ , where  $J_1, J_2 : \mathbb{R}^N \rightarrow (-\infty, +\infty]$  are proper, closed convex functions, it is well known that the nested PPA

$$x^{(k+1)} = \text{prox}_{\lambda J_2} \left( \text{prox}_{\lambda J_1} (x^{(k)}) \right)$$

converges for any fixed parameter  $\lambda > 0$  to a fixed point of  $\text{prox}_{\lambda J_2} \circ \text{prox}_{\lambda J_1}$ . Unfortunately this fixed point is not a minimizer of  $J$  but of  $J_2 + \lambda J_1$ , where  $\lambda J_1$  denotes the Moreau envelope of  $J_1$ . Convergence to the correct minimizer can be achieved by choosing an iteration dependent sequence  $\{\lambda_k\}_k$  fulfilling

$$\sum_{k=0}^{\infty} \lambda_k = \infty, \quad \text{and} \quad \sum_{k=0}^{\infty} \lambda_k^2 < \infty,$$

see [3, 8]. A specific splitting of our inpainting model (3) for the CPPA is given in the appendix.

## 5 Numerical Results

For the numerical computations of the following examples, the presented algorithms were implemented in MATLAB. The experiments were performed on a MacBook Pro with an Intel Quad Core i5, 2.6 Ghz and 8 GB of RAM on OS X 10.9.2.

**Interpolation and Approximation.** As a first example we consider an synthetic SAR data sample taken from [24]<sup>1</sup>, see Fig. 2 (a). We destroy about 89.8% of the data by removing all but the rows and columns that are not divisible by 3, see Fig. 2 (b). This is taken as input for the CPPA in order to minimize (3) using the parameters  $\alpha = (1, 1, 0, 0)^T$ ,  $\beta = (1, 1)^T$  and  $\gamma = 1$ . The result is shown in Fig. 2 (c), where the linear parts are reconstructed perfectly, while the edges are interpolated and hence suffer from linearization of the original circular edge path. The runtime is about 80 seconds for the image of size  $257 \times 257$  pixel when using  $k = 700$  iterations as a stopping criterion for the CPPA from Sec. 4.

**Inpainting for Restoring Image Regions.** A main application of inpainting is to restore destroyed image regions in noiseless images. We use the first model (3) and consider an example

<sup>1</sup>online available at [ftp://ftp.wiley.com/public/sci\\_tech\\_med/phase\\_unwrapping/data.zip](ftp://ftp.wiley.com/public/sci_tech_med/phase_unwrapping/data.zip).

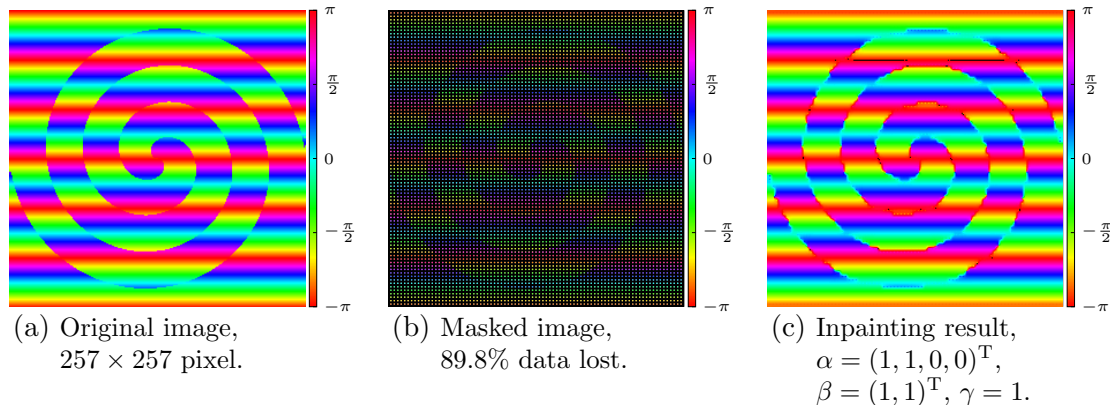


**Figure 2.** The synthetic SAR data in (a) is reduced by a factor of nine by removing two thirds of all rows and columns. They are indicated as black pixels in (b), the right image (c) shows the reconstruction based on first and second order cyclic differences.

adapted from [40], where a similar image was used to demonstrate regularization with a second order model for real valued images. We extend their experiment by including a region with linear increase that is wrapped twice, cf. Fig. 3 (a). We remove a vertical strip in the middle of both regions and stripes between the fore- and background. Furthermore for the second, linearly increasing region we mask a small band in the middle, cf. Fig. 3 (b).

We then employ a real valued inpainting using first and second order differences, cf. Fig. 3 (c). The constant rectangle shows a similar behavior to [40], where the smoothing at the top and bottom is reduced here. This is due to employment of both first and second order real valued differences. Most noticeably, the linearly increasing region is not reconstructed.

The Figs. 3 (d)–(f) illustrate the effects of first and second order absolute cyclic differences. Fig. 3 (d) uses only the first order model, (e) only the second order differences. and (f) combines both. The first order absolute cyclic differences reconstruct the constant region perfectly, but also produce the well known staircasing in the lower part. The second order cyclic model introduces a smooth transition between fore- and background. However, it perfectly reconstructs the linear increase. Combining both the first and second order cyclic models yields a perfect reconstruction of the linearly increasing region while reducing the smooth transition, cf. Fig. 3 (f).

As a second reconstruction example we consider the function  $\text{atan2}(y, x)$  sampled on a regular grid in  $[-\frac{1}{2}, \frac{1}{2}]^2$  having 128 sampling points in each dimension, cf. Fig. 4 (a). We take a circular mask in the center of the image, see Figure 4 (b), where the mask is shown in black. In this experiment we compare the results using only first order absolute cyclic differences with a combined approach of first and second order cyclic model.

When only using first order differences, we obtain a result that again reveals staircasing, cf. Fig. 4 (c). It prefers  $x$ - and  $y$ -axis, and both diagonals, which can be seen by the crosses created in the middle. By also including second order differences we obtain almost the original image, cf. Fig. 4 (d).

For both examples the computation takes about 43 seconds for first order differences and 55 seconds for the combined cases, respectively. We used  $k = 2000$  iterations as a stopping criterion for the CPPA from Sec. 4.

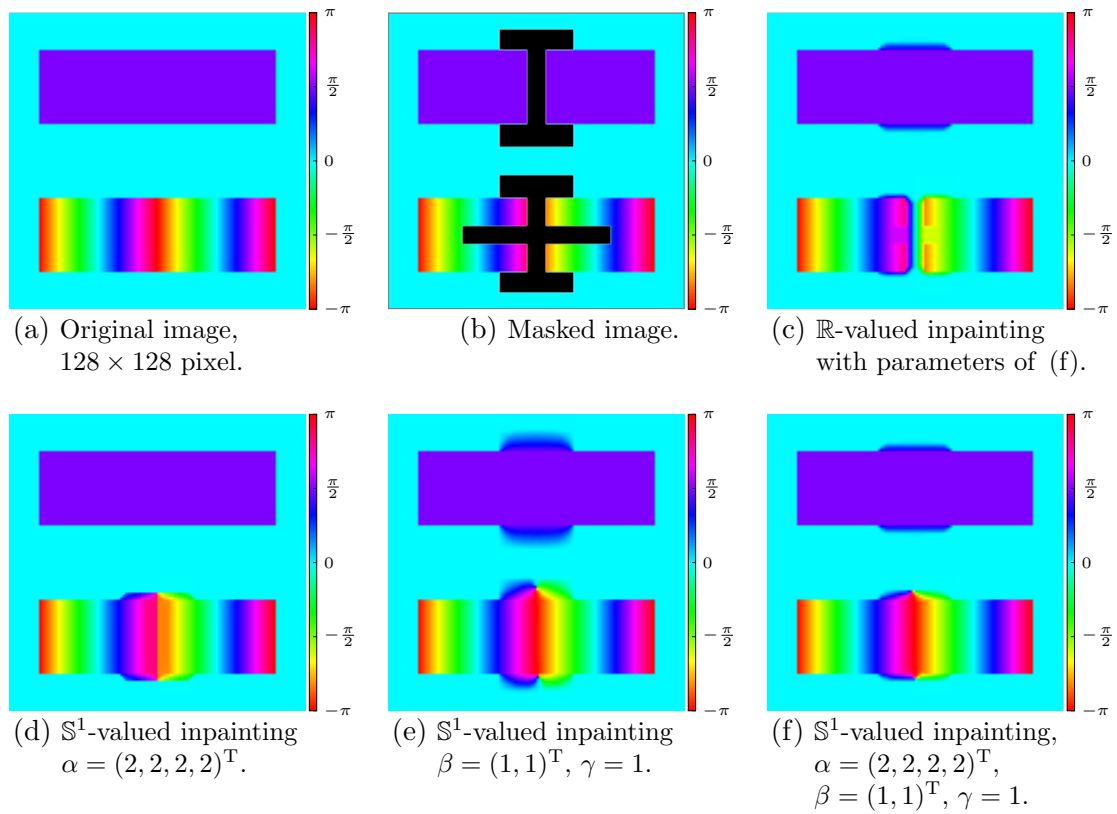


**Figure 3.** Inpainting with first and second order differences: (a) from the original image (b) some parts (black) are lost. (c) A real-valued inpainting fails; (d) a first order model reconstructs the constant region perfectly; (e) a pure second order model has linear artifacts; (f) a first and second order model performs best.



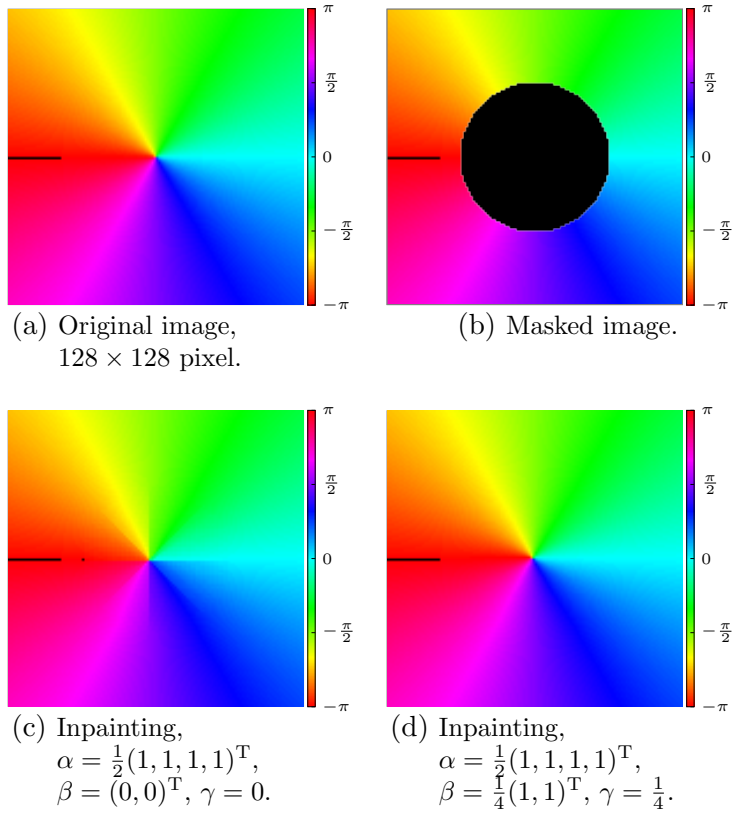


**Figure 4.** We mask a circular region at the center of (a), see (b). The reconstruction used in (c) employs only first order cyclic differences and produces staircasing. Combining first and second order cyclic differences in (d) we obtain a nearly perfect reconstruction.

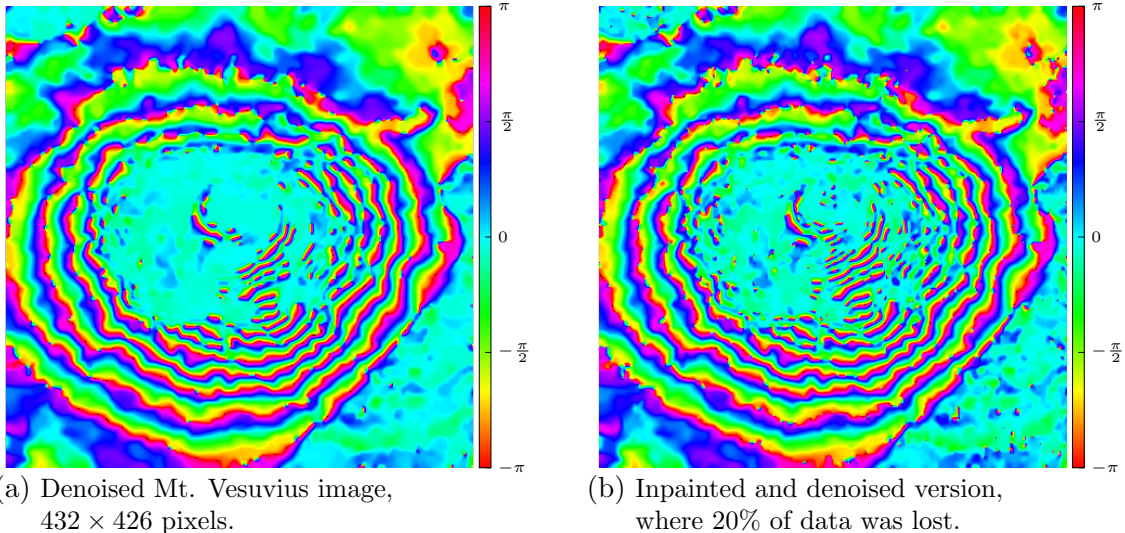


**Figure 5.** Real data of Mount Vesuvius. We compare a pure denoising approach in (a) with a combined inpainting and denoising approach in (b), where 20% of the data was lost before the inpainting and denoising process.

**Inpainting in the presence of noise.** In real world measurements data are often noisy. If these data are also partially lost, we employ the model (4). As an example we consider the measurement of elevation using InSAR [11, 39]. In particular, we consider phase valued measured data of Mount Vesuvius [43]<sup>2</sup>. We compare denoising with simultaneously inpainting and denoising. To this end, we randomly destroyed 20% of the data items. The results without and with lost data are shown in Fig. 5 ((a)) and ((b)), respectively. For the inpainting version the parameters used in Fig. 5 ((a)),  $\alpha = \frac{1}{4}(1, 1, 1, 1)^T$ ,  $\beta = \frac{3}{4}(1, 1)^T$  and  $\gamma = \frac{3}{4}$ , were multiplied by 2. The combined approach of simultaneously inpainting and denoising introduces a few more artifacts than pure denoising; cf. the middle and top right area. However, both results are of comparable quality in smooth regions, e.g., the plateau in the bottom left.

## 6 Conclusions

We proposed an inpainting model for cyclic data which involves our recently established second order cyclic differences. Since there are analytical expressions for the proximal mappings of these differences we suggested a CPP algorithm together with a strategy for choosing the cycles to compute a minimizer of the corresponding functionals efficiently. There is large room for improvements and future work.

We want to apply our second order cyclic differences to other image restoration tasks such as, e.g., deblurring and investigate other couplings of first and second order differences. It is possible to generalize our geometrically driven definition of second order differences to higher dimensional spheres and also to general manifolds. We want to use such generalization for image processing tasks of general manifold-valued data.

<sup>2</sup>online available at <https://earth.esa.int/workshops/ers97/program-details/speeches/rocca-et-al/>

## Appendix

The proximal mappings from Theorem 2.1 can be efficiently applied in parallel if they act on distinct data. This reduces the cycle length  $c$  of the CPPA from Sec. 4 tremendously and provides an efficient, parallel implementation. Especially, the cycle length is independent of the inpainting area  $\Omega$  or the image domain  $\Omega_0$  and depends only on the number of dissimilar differences used. We present a specific splitting in the CPPA of our inpainting model (3) given by

$$J(x) = \alpha \text{TV}_1^\Omega(x) + \beta \text{TV}_2^\Omega(x) + \gamma \text{TV}_{1,1}^\Omega(x)$$

with the constraints  $x_{i,j} = f_{i,j}$  on  $\bar{\Omega}$ . We write

$$J = \sum_{l=1}^{18} J_l$$

with summands  $J_l$  given by the subsequent explanation. We start with the  $\alpha \text{TV}_1^\Omega(x)$  term and first consider the horizontal summand  $\alpha_1 \sum_{(i,j)} d(x_{i,j}, x_{i+1,j})$ . We split this sum into an even and an odd part  $J_1$  and  $J_2$ , more precisely

$$\alpha_1 \sum_{(i,j)} d(x_{i,j}, x_{i+1,j}) = J_1 + J_2,$$

where

$$J_1 + J_2 := \alpha_1 \sum_{(i,j)} d(x_{2i,j}, x_{2i+1,j}) + \alpha_1 \sum_{(i,j)} d(x_{2i+1,j}, x_{2i+2,j}),$$

with the restriction to the summands as in Sec. 3. This means, that for each item  $(i, j)$  in the sum, the corresponding index of at least one of the arguments  $x_{2i,j}, x_{2i+1,j}$  is in  $\Omega$ . For the vertical as well as for the diagonal summands in  $\alpha \text{TV}_1^\Omega(x)$  we proceed analogously to obtain the splitting functionals  $J_3, \dots, J_8$ .

Next, we consider the  $\beta \text{TV}_2^\Omega(x)$  term with its first (horizontal) summand given by  $\beta_1 \sum_{(i,j)} d_2(x_{i-1,j}, x_{i,j}, x_{i+1,j})$ . We decompose this summand into three sums  $J_9, J_{10}, J_{11}$  given by

$$J_9 = \beta_1 \sum_{(i,j)} d_2(x_{3i-1,j}, x_{3i,j}, x_{3i+1,j}),$$

$$J_{10} = \beta_1 \sum_{(i,j)} d_2(x_{3i,j}, x_{3i+1,j}, x_{3i+2,j}),$$

$$J_{11} = \beta_1 \sum_{(i,j)} d_2(x_{3i+1,j}, x_{3i+2,j}, x_{3i+3,j}),$$

again, with the restriction to the summands as in Sec. 3. For the vertical summand in  $\beta \text{TV}_2^\Omega(x)$  we proceed analogously to obtain  $J_{12}, \dots, J_{14}$ .

It remains to split the term  $\gamma \text{TV}_{1,1}^\Omega(x)$  into four functionals  $J_{15}, \dots, J_{18}$  as follows

$$\begin{aligned} J_{15} &= \gamma \sum_{(i,j)} d_{1,1}(x_{2i,2j}, x_{2i+1,2j}, x_{2i,2j+1}, x_{2i+1,2j+1}), \\ J_{16} &= \gamma \sum_{(i,j)} d_{1,1}(x_{2i+1,2j}, x_{2i+2,2j}, x_{2i+1,2j+1}, x_{2i+2,2j+1}), \\ J_{17} &= \gamma \sum_{(i,j)} d_{1,1}(x_{2i,2j+1}, x_{2i+1,2j+1}, x_{2i,2j+2}, x_{2i+1,2j+2}), \\ J_{18} &= \gamma \sum_{(i,j)} d_{1,1}(x_{2i+1,2j+1}, x_{2i+2,2j+1}, x_{2i+1,2j+2}, x_{2i+2,2j+2}). \end{aligned}$$

Each summation is again restricted to those terms where at least one index of an argument of  $d_{1,1}$  is in  $\Omega$ . For  $J_1, \dots, J_{18}$  the corresponding proximal mapping can be explicitly computed and the cycle length  $c = 18$  is independent of the cardinality of  $\Omega$  or  $\Omega_0$ . After application of the proximal mapping of each  $J_i$  we set  $x_{i,j} = f_{i,j}$  on  $\bar{\Omega}$  to fulfill the respective constraint, which is the same as performing a projection.

## References

- [1] M. Almeida and M. Figueiredo. Deconvolving images with unknown boundaries using the alternating direction method of multipliers. *IEEE Trans. on Image Process.*, 22(8):3074–3086, 2013.
- [2] M. Bačák. The proximal point algorithm in metric spaces. *Isr. J. Math.*, 194(2):689–701, 2013.
- [3] M. Bačák. Computing medians and means in Hadamard spaces. *SIAM J. Optim.*, 2014. to appear.
- [4] C. Ballester, M. Bertalmio, V. Caselles, G. Sapiro, and J. Verdera. Filling in by joint interpolation of vector fields and gray levels. *IEEE Trans. Image Process.*, 10(8):1200–1211, 2001.
- [5] R. Bergmann, F. Laus, G. Steidl, and A. Weinmann. Second order differences of cyclic data and applications in variational denoising. *Preprint*, 2014.
- [6] M. Bertalmío, G. Sapiro, V. Caselles, and C. Ballester. Image inpainting. In *Proceedings of SIGGRAPH 2000*, pages 417–424, New Orleans, USA, 2000.
- [7] D. P. Bertsekas. Incremental gradient, subgradient, and proximal methods for convex optimization: a survey. Technical Report LIDS-P-2848, Laboratory for Information and Decision Systems, MIT, Cambridge, MA, 2010.
- [8] D. P. Bertsekas. Incremental proximal methods for large scale convex optimization. *Math. Program., Ser. B*, 129(2):163–195, 2011.
- [9] K. Bredies, K. Kunisch, and T. Pock. Total generalized variation. *SIAM J. Imaging Sci.*, 3(3):1–42, 2009.

- [10] A. Bugeau, M. Bertalmío, V. Caselles, and G. Sapiro. A comprehensive framework for image inpainting. *IEEE Trans. Signal Process.*, 19:2634–2645, 2010.
- [11] R. Bürgmann, P. A. Rosen, and E. J. Fielding. Synthetic aperture radar interferometry to measure earth’s surface topography and its deformation. *Annu. Rev. Earth Planet. Sci.*, 28(1):169–209, 2000.
- [12] J.-F. Cai, B. Dong, S. Osher, and Z. Shen. Image restoration: Total variation, wavelet frames, and beyond. *J. Amer. Math. Soc.*, 25(4):1033–1089, 2012.
- [13] V. Caselles, J.-M. Morel, and C. Sbert. An axiomatic approach to image interpolation. *IEEE Trans. on Image Process.*, 7(3):376–386, 1998.
- [14] A. Chambolle and P.-L. Lions. Image recovery via total variation minimization and related problems. *Numer. Math.*, 76(2):167–188, 1997.
- [15] T. Chan and J. Shen. Local inpainting models and TV inpainting. *SIAM J. Appl. Math.*, 62(3):1019–1043, 2001.
- [16] T. F. Chan, A. Marquina, and P. Mulet. High-order total variation-based image restoration. *SIAM J. Sci. Comput.*, 22(2):503–516, 2000.
- [17] T. F. Chan and J. Shen. *Image Processing and Analysis: Variational, PDE, Wavelet, and Stochastic Methods*. SIAM, 2005.
- [18] C. Ched’Hotel, D. Tschumperlé, R. Deriche, and O. Faugeras. Regularizing flows for constrained matrix-valued images. *J. Math. Imaging Vis.*, 20(1-2):147–162, 2004.
- [19] S. Didas, J. Weickert, and B. Burgeth. Properties of higher order nonlinear diffusion filtering. *J. Math. Imaging Vis.*, 35:208–226, 2009.
- [20] O. P. Ferreira and P. R. Oliveira. Proximal point algorithm on Riemannian manifolds. *Optimization*, 51(2):257–270, 2002.
- [21] N. I. Fisher. *Statistical Analysis of Circular Data*. Cambridge University Press, 1995.
- [22] P. Fletcher. Geodesic regression and the theory of least squares on Riemannian manifolds. *Int. J. Comput. Vision*, 105(2):171–185, 2013.
- [23] P. Fletcher and S. Joshi. Riemannian geometry for the statistical analysis of diffusion tensor data. *Signal Process.*, 87(2):250–262, 2007.
- [24] D. C. Ghiglia and M. D. Pritt. *Two-dimensional phase unwrapping: theory, algorithms, and software*. Wiley, 1998.
- [25] M. Giaquinta, G. Modica, and J. Souček. Variational problems for maps of bounded variation with values in  $S^1$ . *Calc. Var.*, 1(1):87–121, 1993.
- [26] M. Giaquinta and D. Mucci. The BV-energy of maps into a manifold: relaxation and density results. *Ann. Sc. Norm. Super. Pisa Cl. Sci.*, 5(4):483–548, 2006.
- [27] M. Giaquinta and D. Mucci. Maps of bounded variation with values into a manifold: total variation and relaxed energy. *Pure Appl. Math. Q.*, 3(2):513–538, 2007.

- [28] P. Grohs, H. Hardering, and O. Sander. Optimal a priori discretization error bounds for geodesic finite elements. Technical Report 2013-16, Seminar for Applied Mathematics, ETH Zürich, Switzerland, 2013.
- [29] P. Grohs and J. Wallner. Interpolatory wavelets for manifold-valued data. *Appl. Comput. Harmon. Anal.*, 27(3):325–333, 2009.
- [30] C. Guillemot and O. Le Meur. Image inpainting: Overview and recent advances. *IEEE Signal Process. Mag.*, 31(1):127–144, 2014.
- [31] W. Hinterberger and O. Scherzer. Variational methods on the space of functions of bounded Hessian for convexification and denoising. *Computing*, 76(1):109–133, 2006.
- [32] S. R. Jammalamadaka and A. SenGupta. *Topics in Circular Statistics*. World Scientific Publishing Company, 2001.
- [33] S. Lefkimmiatis, A. Bourquard, and M. Unser. Hessian-based norm regularization for image restoration with biomedical applications. *IEEE Trans. Image Process.*, 21(3):983–995, 2012.
- [34] J. Lellmann, E. Strekalovskiy, S. Koetter, and D. Cremers. Total variation regularization for functions with values in a manifold. In *IEEE ICCV 2013*, pages 2944–2951, 2013.
- [35] M. Lysaker, A. Lundervold, and X.-C. Tai. Noise removal using fourth-order partial differential equations with applications to medical magnetic resonance images in space and time. *IEEE Trans. Image Process.*, 12(12):1579–1590, 2003.
- [36] T. März. Image inpainting based on coherence transport with adapted distance functions. *SIAM J. Imaging Sci.*, 4(4):981–1000, 2011.
- [37] T. März. A well-posedness framework for inpainting based on coherence transport. *Found. Comput. Math.*, 2014. to appear.
- [38] S. Masnou and J.-M. Morel. Level lines based disocclusion. In *IEEE ICIP 1998*, pages 259–263, 1998.
- [39] D. Massonnet and K. L. Feigl. Radar interferometry and its application to changes in the Earth’s surface. *Rev. Geophys.*, 36(4):441–500, 1998.
- [40] K. Papafitsoros and C. B. Schönlieb. A combined first and second order variational approach for image reconstruction. *J. Math. Imaging Vis.*, 2(48):308–338, 2014.
- [41] X. Pennec. Intrinsic statistics on Riemannian manifolds: Basic tools for geometric measurements. *J. Math. Imaging Vis.*, 25(1):127–154, 2006.
- [42] I. U. Rahman, I. Drori, V. C. Stodden, and D. L. Donoho. Multiscale representations for manifold-valued data. *Multiscale Model. Simul.*, 4(4):1201–1232, 2005.
- [43] F. Rocca, C. Prati, and A. M. Guarnieri. Possibilities and limits of SAR interferometry. In *Proc. Int. Conf. Image Process. Techn. 1996*, pages 15–26, 1997.
- [44] R. T. Rockafellar. Monotone operators and the proximal point algorithm. *SIAM J. Control Optim.*, 14(5):877–898, 1976.

- [45] L. I. Rudin, S. Osher, and E. Fatemi. Nonlinear total variation based noise removal algorithms. *Physica D.*, 60(1):259–268, 1992.
- [46] O. Scherzer. Denoising with higher order derivatives of bounded variation and an application to parameter estimation. *Computing*, 60:1–27, 1998.
- [47] S. Setzer and G. Steidl. Variational methods with higher order derivatives in image processing. In *Approximation Theory XII: San Antonio 2007*, pages 360–385, 2008.
- [48] S. Setzer, G. Steidl, and T. Teuber. Infimal convolution regularizations with discrete l1-type functionals. *Commun. Math. Sci.*, 9(3):797–872, 2011.
- [49] E. Strelakovski and D. Cremers. Total variation for cyclic structures: Convex relaxation and efficient minimization. In *IEEE CVPR 2011*, pages 1905–1911, 2011.
- [50] E. Strelakovski and D. Cremers. Total cyclic variation and generalizations. *J. Math. Imaging Vis.*, 47(3):258–277, 2013.
- [51] T. Valkonen, K. Bredies, and F. Knoll. Total generalized variation in diffusion tensor imaging. *SIAM J. Imag. Sci.*, 6(1):487–525, 2013.
- [52] A. Weinmann. Interpolatory multiscale representation for functions between manifolds. *SIAM J. Math. Anal.*, 44(1):162–191, 2012.
- [53] A. Weinmann, L. Demaret, and M. Storath. Total variation regularization for manifold-valued data. *Preprint*, 2013.